**Atmospheric
Chemistry
and Physics
Discussions**

Performance evaluation of a high-resolution parallel-plate differential mobility analyzer

J. P. Santos[1], E. Hontañón[1], E. Ramiro[1], and M. Alonso[2]

[1]RAMEM S.A., Sambara 33, 28027 Madrid, Spain
[2]National Center for Metallurgical Research (CENIM-CSIC), Avda. Gregorio del Amo 8, 28040 Madrid, Spain

Correspondence to: J. P. Santos (jpsantos@ramem.com)

ACPD

8, 17631–17660, 2008

High resolution parallel plate DMA

J. P. Santos et al.

Title Page

Abstract	Introduction
Conclusions	References
Tables	Figures

|◄ | ►|

◄ | ►

Back | Close

Full Screen / Esc

Printer-friendly Version

Interactive Discussion

Abstract

A high-resolution differential mobility analyzer (DMA), specially designed for

  (i) the measurement of ion mobility spectra, and

  (ii) the generation of a continuous stream of monomobile ions,

has been developed and tested. The apparatus consists of two parallel-plate electrodes between which an electric field is applied. The test ion stream flows into the instrument through a narrow rectangular slit made in one of the electrodes, and migrates toward the other electrode driven by the applied field, while being transported by a stream of clean air which flows parallel to the plates at Reynolds number between 2×10^4 and 9×10^4 in laminar flow conditions. The collector electrode contains also a narrow slit through which ions of the desired mobility are withdrawn out of DMA. The classified ion current is measured with a high-sensitivity electrometer having a noise level around 0.1 fA.

    The theory behind the DMA operation is first discussed, focusing on the special case of parallel-plate geometry. Some generic results showing the stability and repeatability of the measurements and the resolving power of the instrument are presented next. The last part of the paper deals with the application of the apparatus to the study of the effect of humidity and aging time on the mobility spectra of air ions generated by a low-activity ^{241}Am source.

1 Introduction

The mobility of a cluster ion can provide information about its structure and geometry; for instance, geometric isomers can be resolved on the basis of their different mobilities (Zarpas et al., 1986, 1988). Ion mobility spectrometry has been used to detect drugs, explosives, chemical warfare agents and other ambient pollutants (Chen et al., 1996; Swing et al., 2001; Hill and Martin, 2002; Buryakov, 2004; Vautz et al., 2006).

Traditionally, ion mobility measurements have been performed in drift tubes, containing a buffer gas (maintained at either very low or atmospheric pressure) and a series of electrodes to provide a uniform electric field (Clemmer and Jarrold, 1997). In these instruments, mobility is inferred from the measure time required for an ion to traverse the length of the drift tube.

An alternative instrument to measure ion mobility at atmospheric pressure is the so called differential mobility analyzer (DMA), in which the ions migrate between two electrodes held at different constant potentials while been transported by a stream of gas (initially clean) flowing parallel to the electrodes. The long history of differential mobility analyzers can be traced back to the early works of Zeleny and Langevin using coaxial cylindrical condensers to measure the mobility of air ions. These works, as well as later developments that followed, have been extensively described in a review article of Flagan (1998). In all these early works, the DMA resolution was relatively poor, so that ions with similar mobilities could not be properly resolved.

DMAs later evolved into somewhat longer coaxial cylindrical columns able to measure the mobility of larger aerosol particles and, at the same time, to classify aerosols according to their size. There are two main types of coaxial DMAs, which can be termed single-channel and multi-channel analyzers. In the single-channel DMA, the sampled aerosol exits the apparatus through an outlet slit; the number concentration of the classified particles can then be measured using either an electrometer or a particle counter. By varying the electric field between the electrodes, particles of different mobilities are sequentially classified. In this manner, the mobility distribution of the aerosol population can be measured, and can later be transformed into the corresponding particle size distribution provided the charge distribution on the particles is known. The typical prototype of single-channel, coaxial cylindrical DMA was developed in the 1960s at the University of Minnesota (Whitby and Clark, 1966; Knutson and Whitby, 1975).

In the multi-channel design, one of the electrodes is equipped with a series of insulated metal rings, each connected to its own electrometer. When a certain electric field

J. P. Santos et al.

is applied between the coaxial electrodes, the charged particles of a given polarity are deposited differentially onto the metal rings. This arrangement allows for the simultaneous measurement of the number concentration of particles having different mobility, thus reducing considerably the time required for the measurement of the entire mobility distribution. The multi-channel analyzer, which is specially indicated for rapidly fluctuating aerosols, was developed in the 1970s at the University of Tartu (Tammet, 1970; Tammet et al., 2002).

Perhaps the main advantage of the single-channel DMA over multi-channel analyzers and drift tubes is, besides its lower cost, the possibility to use it to generate a continuous stream of monodisperse aerosol particles or monomobile ions. The particles or ions of the desired mobility can subsequently be employed to perform a great variety of fundamental and applied investigations (ion clustering, chemical kinetics, particle size growth by condensation or coagulation, size-dependent electrical behavior, filtration, and many others). (In the rest of this article, we will always have in mind single-channel analyzers, and will refer to them simply as DMAs, omitting the "single-channel" term.)

During the last fifteen years, a great effort has been addressed to the improvement of the performance of DMAs, mainly modifying the aerosol inlet geometry in order to reduce diffusional deposition losses (Winklmayr et al. 1991; Chen et al., 1999), and shortening the mean aerosol residence time by minimizing the column length (Rosell-Llompart et al., 1996) and operating the DMA in laminar flow conditions with sheath gas flow at high Reynolds for classifying ions with high resolution (de Juan and Fernández de la Mora, 1998). Also, two new conceptions of analyzers have appeared, one in which an additional electric field parallel to the main gas flow is applied (Loscertales, 1998), and other type of DMA incorporating an electrified screen which permits maintaining the electrodes containing the inlet and outlet slits at the same potential (Martínez-Lozano et al., 2006), thus preventing electrophoretic losses.

All the above mentioned improvements were implemented in concentric cylindrical DMAs. With this geometry, electrode centering is critical to the performance of a DMA; even a very small misalignment of the electrodes can lead to a severe deterioration

of the resolving power of the instrument. To avoid this difficulty, we have preferred to redesign the DMA using a parallel-plate geometry, so that electrode centering is no longer an issue. Furthermore, mechanical machining and positioning of the electrodes are both easier (thereby reducing the cost) and more precise.

5   There is still an additional reason for choosing the parallel-plate geometry, related to the strong Brownian motion of nanoparticles and ions. In general, the Brownian motion makes the particles or ions to deviate from their otherwise deterministic trajectories given by the electric and gas flow velocity fields. As a consequence, the trajectories of different-mobility particles mix up and the instrument resolution deteriorates. The

10   extent of Brownian dispersion depends on the uniformity of the electric field and on the average direction of particle motion in the field (Alonso, 2002; Song and Dhaniyala, 2007). Thus, if particles move in the direction of increasing electric field strength, which is the usual case in cylindrical DMAs, the resolution worsens because the variance of the distribution of particle positions is larger than for a free particle, i.e. larger than $2Dt$

15   (D is the particle or ion diffusion coefficient, and t is its mean residence time between the inlet and outlet slits). If the electric field is uniform, as in the parallel-plate geometry, the variance is exactly $2Dt$ an, hence, the resolution of our proposed mobility analyzer is better than that attainable with a conventional coaxial cylindrical DMA.

     In this work, the novel high-resolution DMA recently developed by us is described

20   in some detail. The electro-fluid-dynamical equations behind the DMA operation will be presented for the specific design of our instrument. Next, the repeatability and stability of the mobility distribution measurements and the resolving power of the DMA will be discussed. The final section of the article will deal with an illustrative application of our DMA: the examination of the effect of humidity and aging time on the mobility

25   distribution of laboratory air ions generated by a [241]Am radioactive source.

2   Description of the instrument

A sketch of the proposed DMA (RAMEM IONER X1) (Ramiro and Rivero, 2007) is shown in Fig. 1a. The DMA proper, i.e. the classification zone comprising the space delimited by the parallel-plate electrodes and the inlet and outlet slits, is inserted within a closed-circuit rectangular duct in which a sheath gas (usually air) flows. The separation between the electrodes is 5 mm, the distance from the ion inlet slit to the ion outlet slit is also 5 mm and the width of the classification region is 10 mm. The Reynolds number of the flow in the classification region ranges from 2×10^4 to 9×10^4 (flow rates between 200 and 900 l min^{-1}). In spite of these unusually high Reynolds numbers, transition to turbulence could be avoided by means of several stages of laminarizing screens followed by a converging section (trumpet). The screens serve to damp the turbulence of the sheath gas and to spread this uniformly over the flow cross section, while the trumpet helps to stabilize the flow by gradually accelerating it up to the classification zone. The inlet to outlet area ratio of the trumpet is 8. Both features cause a noticeable flow pressure drop which is recovered in a diverging section (diffuser) located downstream of the classification region.

The aerosol of ions (or charged nanoparticles) is continuously fed at a low flow rate (generally, less than 6 l min^{-1}) into the classification zone through a narrow slit. The motion of ions in the classification zone has two components: one parallel to the electrodes, due to the main gas flow; and another one, driven by the applied electric field, directed toward the collector electrode. The latter contains also a slit through which ions having mobility within a narrow range are withdrawn from the loop circuit. The mobility of the thus classified ions depends on the sheath (main) gas flow rate and the strength of the electric field.

If the classified ions are allowed to leave the DMA through the outlet port, the instrument works as a generator of monomobile ions. The possibility of employing this instrument as a stable, continuous source of well-characterized ions is, as commented above, a great advantage of DMAs over time-of-flight mobility spectrometers.

If, on the contrary, one wishes to determine the mobility distribution of the fed ion stream, a metal rod connected to a high-sensitivity electrometer (RAMEM IONER EL-5010) is placed just behind the outlet slit, to measure the current carried by the ions classified at progressively increasing values of the applied electric field.

The dimensions of the inlet and outlet slits can be changed at will. For the experimental work discussed below, we have used rectangular inlet and oulet slits 6 mm in length and 120 μm in width.

At a given value of the applied voltage between the electrodes, only a fraction of ions can at most be classified and withdrawn from the DMA; the rest of the ion population leaves the classification zone with the main gas flow. A fraction of these unclassified, excess ions will progressively be lost by diffusion to the inner walls of the loop circuit, but a certain finite fraction of ions will survive and end up again in the classification zone. A steady buildup of excess ions in the loop would lead to increasing noise in the measured currents. To avoid this undesired effect, the loop duct is equipped with a small electrostatic precipitator downstream of the classification zone, to remove the unclassified ions.

The sheath gas loop circuit is also equipped with a Venturi-type flowmeter (McCrometer V-Cone), placed upstream of the classification zone. Pressure and temperature are also measured in the section containing the flowmeter. The actual sheath flow rate in the classification zone is calculated from the values of pressure, temperature and flow rate measured upstream, assuming isentropic flow conditions. It will be shown below that this assumption is fully justified. A layout of the ion differential mobility analyzer IONER X1 is depicted in Fig. 1b.

2.1 Ideal operation of the parallel-plate DMA

The operation of a DMA is described by its transfer function $\Omega(k, V)$, which is defined as the probability that an ion of mobility k is classified through the outlet slit when a voltage difference V is applied between the electrodes. To calculate the transfer function of the instrument there exists a standard method, first proposed by Knutson

and Whitby (1975) for the cylindrical DMA, and which will be summarized here for the parallel-plate geometry.

The equation of motion for the ion of mobility k is

$$\frac{d\mathbf{r}}{dt}=\mathbf{u}+k\mathbf{E},\tag{1}$$

5   where $\mathbf{r}$ is the ion position vector, $\mathbf{u}$ the gas flow velocity, and $\mathbf{E}$ the applied electric field. The main gas stream flows in the x direction, and the electric field is directed along the y-coordinate, normal to the electrodes. Hence, Eq. (1) reduces to

$$\frac{dx}{dt}=u_x;\quad \frac{dy}{dt}=kE_y.\tag{2}$$

Next, the stream function ψ is defined by means of the relations

10   $$u_x=-\frac{1}{\Delta_z}\frac{\partial\psi}{\partial y};\quad u_y=-\frac{1}{\Delta_z}\frac{\partial\psi}{\partial x},\tag{3}$$

where Δ_z is the DMA width. The latter is assumed to be sufficiently large so that the flow velocity u_x depends only on y. In writing Eq. (3) it has been further assumed that the flow is incompressible in the classification zone, i.e. $\nabla.\mathbf{u}=0$. Hence,

$$\psi=-\Delta_z\int u_x dy.\tag{4}$$

15   By analogy to ψ, we introduce the function

$$\phi=\Delta_z\int E_y dx,\tag{5}$$

which may be called the electric flux function.

Consider now the expression $T=\psi+k\phi$, and form its substantial derivative following the ion trajectory:

20   $$\frac{DT}{Dt}=\frac{\partial T}{\partial t}+\frac{dx}{dt}\frac{\partial T}{\partial x}+\frac{dy}{dt}\frac{\partial T}{\partial y}.\tag{6}$$

High resolution parallel plate DMA

J. P. Santos et al.

Printer-friendly Version

Interactive Discussion

For steady-state DMA operation, $\partial T/\partial t = 0$. The last two terms in Eq. (6) cancel each other because of Eqs. (2), (4) and (5). Therefore,

$$T = \psi + k\phi = \text{const}. \tag{7}$$

along the ion trajectory.

5   In the classified stream withdrawn through the outlet slit there will appear ions with mobility distributed within two extreme values, which will be denoted as k_{min} and k_{max}. These can be determined considering the boundary streamlines shown schematically in Fig. 2.

In the normal operation of the DMA, the flow rate of the incoming aerosol matches
10   the flow rate of the classified stream, Q_a and, likewise, the flow rates of the sheath gas entering and exiting the classification zone are equal to each other, and will be denoted as Q_{sh}. According to Eq. (4), the flow bounded by any two streamlines ψ_i and ψ_k is given by the difference $\psi_i - \psi_k$. Therefore, we can write

$$Q_a = \psi_1 - \psi_2 = \psi_3 - \psi_4, \tag{8}$$

15   $$Q_{sh} = \psi_2 - \psi_4 = \psi_1 - \psi_3. \tag{9}$$

The ion with minimum mobility which appears in the classified stream is that which enters the classification zone with streamline ψ_2 and is withdrawn along streamline ψ_3. For this ion, Eq. (7) becomes

$$\psi_2 + k_{min}\phi_{in} = \psi_3 + k_{min}\phi_{out},$$

20   from where

$$k_{min} = \frac{\psi_2 - \psi_3}{\phi_{out} - \phi_{in}}. \tag{10}$$

Neglecting edge effects in the electric field, we can write

$$\phi_{out} - \phi_{in} = \frac{\Delta_x \Delta_z}{\Delta_y} V, \tag{11}$$

where V is the voltage applied between the electrodes, Δ_y is the separation distance between the electrodes, and Δ_x is the distance between the inlet and outlet slits measured along the x-direction. Substituting Eq. (11) into Eq. (10), and taking Eqs. (8) and (9) into account, we arrive at

$$k_{min} = \frac{\Delta_y}{\Delta_x \Delta_z} \frac{Q_{sh} - Q_a}{V}. \tag{12}$$

In an analogous manner, one can determine the maximum mobility of the classified ions. These enter the DMA with streamline ψ_1 and leave the classification zone along streamline ψ_4. After a few elementary algebraic manipulations, it is found

$$k_{max} = \frac{\Delta_y}{\Delta_x \Delta_z} \frac{Q_{sh} + Q_a}{V}. \tag{13}$$

Finally, the mean mobility of the ions in the classification stream can be determined either repeating the above analysis for streamlines $\psi_{c,in}$ and $\psi_{c,out}$, or simply by taking the arithmetic mean of Eqs. (12) and (13):

$$k_c = \frac{\Delta_y}{\Delta_x \Delta_z} \frac{Q_{sh}}{V}. \tag{14}$$

The normalized full width at half height (FWHH) of the transfer function is then expressed as

$$FWHH_{id} = \frac{\Delta k}{2 k_c} = \frac{k_{max} - k_{min}}{2 k_c} = \frac{Q_a}{Q_{sh}}. \tag{15}$$

The resolution or resolving power of the instrument is defined as the inverse of the relative full width at half height, $R = 1/FWHH$. Thus, in ideal conditions, the resolution is given by the sheath to aerosol flow rate ratio.

At a given applied voltage, all the possible trajectories of an ion of mobility k are bounded by two limiting trajectories, which will be called T_A and T_B. From Eq. (7) we have

$$\psi_{A,in} + k\phi_{in} = \psi_{A,out} + k\phi_{out}, \tag{16}$$

$$\psi_{B,\text{in}} + k\phi_{\text{in}} = \psi_{B,\text{out}} + k\phi_{\text{out}}. \tag{17}$$

Consider again the schematic streamlines drawn in Fig. 2. The boundary trajectories for the ion of mobility k start at the starting points of streamlines ψ_1 and ψ_2, say

$$\psi_{A,\text{in}} = \psi_2, \quad \psi_{B,\text{in}} = \psi_1. \tag{18}$$

With the help of Eq. (11), and Eqs. (15–18), one finds the "outlet" boundary streamlines for this ion of mobility k:

$$\psi_{A,\text{out}} = \psi_2 - \frac{\Delta_x \Delta_z}{\Delta_y} kV, \tag{19}$$

$$\psi_{B,\text{out}} = \psi_1 - \frac{\Delta_x \Delta_z}{\Delta_y} kV. \tag{20}$$

The transfer function can then be evaluated as the fraction of the flow $\psi_{B,\text{out}} - \psi_{A,\text{out}}$ which is common with (or "intersects") the classified flow $\psi_3 - \psi_4$:

$$\Omega = \begin{cases} \frac{\min(\psi_3, \psi_{B,\text{out}}) - \max(\psi_4, \psi_{A,\text{out}})}{\psi_{B,\text{out}} - \psi_{A,\text{out}}} \\ \quad \text{if } \psi_{A,\text{out}} \leq \psi_3 \text{ and } \psi_{B,\text{out}} \geq \psi_4 \\ \quad 0 \text{ elsewhere} \end{cases} \tag{21}$$

The procedure to express Eq. (21) in terms of flow rates and mobilities is purely algebraic and straightforward, but tedious. The final result is

$$\Omega(k, V) = \begin{cases} 1 - \frac{Q_{sh}}{Q_a} \left| 1 - \frac{k}{k_c} \right| & \text{if } k_{\min} \leq k \leq k_{\max} \\ 0 & \text{elsewhere} \end{cases}, \tag{22}$$

where $k_{\min}$, $k_{\max}$ and k_c are given by Eqs. (12–14).

The transfer function (Eq. 22) describes the ideal operation of the DMA. Its shape is a triangle of unit height, symmetric about the central mobility k_c, and with a base width equal to $k_{\max} - k_{\min}$. It is interesting to note that the transfer function (Eq. 22) coincides exactly with that found for concentric cylindrical DMAs (Knutson and Whitby, 1975).

2.2 Diffusion broadening of the transfer function

In real conditions, the transfer function shape is closer to a Gaussian, with height less than unity and base width larger than $k_{max} - k_{min}$, because the strong Brownian motion of the ions prevents them from following the deterministic trajectories given by the simple Eq. (7). The distorting effect of Brownian motion on the shape of the transfer function has been studied by a number of authors (Tammet, 1970; Kousaka et al., 1985; Stolzenburg, 1988; Rosell-Llompart et al., 1996; Hagwood et al., 1999; Salm, 2000).

The quantitative effect of Brownian diffusion on the instrument resolution can be estimated in a particularly simple manner. In the absence of diffusion, an ion follows the trajectory given by the equation of motion (Eq. 2) and arrives at the collector electrode at a certain position x' downstream. When diffusion is taken into account, the arrival position of the ion can be approximated as a Gaussian distribution of mean x' and standard deviation

$$\sigma_{diff} = \frac{\delta}{\Delta_x \cos \alpha},$$
(23)

where $\delta = \sqrt{2Dt}$ is the root mean square displacement about the deterministic trajectory (D=ion diffusion coefficient; t=mean ion residence time in the classification zone), α is the angle formed between this trajectory and the x-axis, and the effective length of the classification zone, Δ_x, has been introduced simply to express σ_{diff} in dimensionless form. Expressing t in terms of the mean axial velocity $\overline{u_x}$ ($t = \Delta_x / \overline{u_x}$), diffusional variance can be written as

$$\sigma_{diff}^2 = \frac{2D}{\overline{u_x}\Delta_x} \frac{\Delta_x^2 + \Delta_y^2}{\Delta_y^2}.$$
(24)

On the other hand, using the Einstein's relation $k = peD/k_BT$ (pe=total charge on the ion; k_B=Boltzmann's constant; T=absolute temperature), and expressing $\overline{u_x}$ in terms

of the flow rates, it is straightforward to find, with the help of Eq. (14), that the relative diffusional variance can be also expressed as

$$\sigma_{\text{diff}}^2 = 4 \frac{k_B T}{peV}. \tag{25}$$

2.3 Combined effect of flow rate ratio and diffusion on the resolution

Since variances are additive, it is possible to estimate the DMA resolution accounting for the combined effect of flow rate ratio and diffusion using the total relative variance

$$\sigma^2 = \sigma_{id}^2 + \sigma_{\text{diff}}^2, \tag{26}$$

with σ_{diff}^2 given by Eq. (15), and

$$\sigma_{id}^2 = \frac{\left\langle k^2 \right\rangle_{id} - \langle k \rangle_{id}^2}{k_c^2} = \frac{1}{6} \left(\frac{\Delta_y}{\Delta_x \Delta_z} \frac{Q_a}{k_c V} \right)^2, \tag{27}$$

where the moments of the classified ions mobility distribution have been calculated as

$$\langle k^m \rangle_{id} = \frac{\displaystyle\int_{k_{\min}}^{k_{\max}} k^m \Omega \, dk}{\displaystyle\int_{k_{\min}}^{k_{\max}} \Omega \, dk}, \tag{28}$$

and Ω is the ideal transfer function given by Eq. (22).

Assuming that the combined transfer function is a Gaussian, the FWHH is related to the standard deviation σ by the formula FWHH$=(8 \ln 2)^{1/2} \sigma$, and one arrives at

$$\text{FWHH} = \left\{ 8 \ln 2 \left[\frac{1}{6} \left(\frac{\Delta_y}{\Delta_x \Delta_z} \frac{Q_a}{k_c V} \right)^2 + 4 \frac{k_B T}{peV} \right] \right\}^{1/2}. \tag{29}$$

High resolution parallel plate DMA

J. P. Santos et al.

Title Page

Abstract	Introduction
Conclusions	References
Tables	Figures

|◄ | ►|

◄ | ►

Back | Close

Full Screen / Esc

Printer-friendly Version

Interactive Discussion

J. P. Santos et al.

Besides Brownian motion, other nonidealities may affect the DMA resolution. Among these, the most important is possibly the width of the ion inlet and outlet slits. Note that in the derivation of the ideal transfer function, what has been considered is the fluid-dynamic dimension of the slits (the withdrawn flow rate) rather than their actual physical dimensions. This is so because in Eq. (11) we have neglected the slit edge effects on the electric field, i.e. we have assumed a constant potential all along $y=0$, and also a constant potential along $y=\Delta_y$, as if the slits were absent. In reality, the electric field "penetrates" into the slits and this will have a measurable effect on ion trajectories (Rosell et al., 1996; Chen et al., 1999). So far, however, no systematic study concerning the effect of the slit width on the resolution has been reported.

It must be noted that nonidealities affect the resolution of the instrument, but not the form of the basic Eq. (14), which gives the centroid mobility of the classified ions when the applied voltage is V, and which remains valid under all circumstances.

3   Performance evaluation

First, a series of measurements were carried out to check the validity of the isentropic flow assumption commented above. Negative air ions generated by passing filtered and dried room air through a corona discharge ionizer (RAMEM IONER CC08010) were fed into the DMA at a constant flow rate of $3 \, \mathrm{l \, min^{-1}}$. The flow rate of sheath air through the DMA was varied between about 200 and $500 \, \mathrm{l \, min^{-1}}$ (as measured by the Venturi-type flowmeter upstream of the classification zone). Some representative spectra are shown in Fig. 3. The sheath flow rates that appear in the legend are those calculated for the classification zone assuming isentropic flow conditions. The spectra are presented as the total ionic current measured by the electrometer placed behind the outlet slit versus the voltage difference applied to the parallel-plate electrodes. Table 1 shows the relevant data for the high-mobility peak, the one marked with an asterisk in Fig. 3. The mobility, calculated with Eq. (14), was transformed into reduced mobility by

using Langevin's rule

$$k_0 = k \left(\frac{P}{760} \right) \left(\frac{273}{273+T} \right), \qquad (30)$$

where P (in mmHg) and T (in K) are, respectively, the calculated pressure and temperature at the classification zone.

As the results in Table 1 show, the reduced mobilities, calculated from spectra obtained at quite different sheath flow rates, agree very well with each other. This example illustrates the degree of accuracy attainable with this spectrometer.

The repeatability of the measurements with the IONER X1 ion mobility analyzer has also proven to be excellent. The operating conditions (sheath and aerosol flow rates, voltage between the parallel-plate electrodes) as well as the electrometer response are very stable, as the data plotted in Fig. 4 shows. The results shown in this plot were obtained by recording the output current for periods of 10, 20 and 30 min, keeping fixed the DMA voltage and flow rates. Filtered and dried room air was passed through a small tube (20 mm long and 4 mm ID) containing two thin disks (⌀5 mm) of ^{241}Am, each one with a nominal activity of 0.9μCi, stuck to the inner wall in diametrically opposite positions. The radioactive ionizer is the same ionizer employed for the measurements whose results were shown above in Fig. 4. It consisted of a circular copper tube, containing two thin disks (⌀5 mm) of ^{241}Am.

The concentrations of positive ions generated by ^{241}Am were quite stable over long periods of time. The electrometer noise was of the order of 0.1 fA. In the case of negative corona air ions, those whose spectra was shown above in Fig. 3, the stability was not as good as for ions generated in the radioactive ionizer, but this is related to the corona ionizer itself rather than to the IONER X1 performance capability.

Experiments were conducted to assess the resolving power of IONER X1 too. In the experiments, ions of a well-defined mobility ($k=0.96\,\text{cm}^2\,\text{V}^{-1}\,\text{s}^{-1}$) were generated by electrospraying a solution of tetraheptylammonium bromide (THAB) in ethanol (10^3 ppm). In that way two singly charged ions of THA, monomer and dimer, having mobilities of 0.96 and $0.67\,\text{cm}^2\,\text{V}^{-1}\,\text{s}^{-1}$ (20°C, 1 atm) are obtained. The ion flow rate

Q_a was maintained constant at $4\,l\,min^{-1}$, while the sheath flow rate Q_{sh} was varied between 200 and $540\,l\,min^{-1}$; the corresponding classification voltage V ranged from 3.5 to 7.8 kV. The ion mobility peaks could be well fitted to Gaussians. The relative full width at half height (FWHH) of the mobility peaks correspondent to the THA monomer is plotted as a function of the classification voltage in Fig. 5; the theoretical values predicted by Eq. (29) are also shown for comparison. Several series of experiments were carried out in which the relative positions of the laminarizing screens were changed with respect to a standard configuration. The best FWHH value of 0.025 (resolution $R=40$) was obtained at the maximum classification voltage ($V=7.8$ kV), while the theory predicts a value of 0.011 ($R=91$). At the sight of these results, new experiments have been initiated in order to figure out the reasons for the non-ideal behaviour of IONER X1, especially the effect of the distorted flow and electric fields in the vicinity of the ion inlet and outlet slits.

4   Applications of the high-resolution differential mobility analyzer

In the final part of this article, we will present the results of some experimental measurements carried out with the aim to illustrate the potential capabilities of this novel instrument. The selected example deals with the effects of air humidity and aging time on the mobility spectra of air ions generated by a radioactive source.

Humid air with known water content was prepared by mixing, in variable proportions, a stream of synthetic air (water content below 3 ppm according to the manufacturer, Air Liquide Alphagaz) with a second stream of synthetic air previously passed through a humidifier operated under controlled conditions of pressure and temperature. The resulting mixture was made to flow through the ^{241}Am ionizer and the DMA.

The volume between the outlet of the ionizer and the inlet slit of the DMA was 1.04 cm^3. The aging time of ions was determined as their mean residence time in this volume. Aging time was varied by modifying the total flow rate of the mixture of dry and humid air passing through the ionizer into the DMA. Experiments were carried out

with water content ranging between 0 (actually <3 ppm) and 40 g/m^3, and mean ion aging time between 10 and 25 ms.

Figures 6 and 7 show the effect of aging time on the mobility distribution of negative and positive air ions at fixed water content. Mobilities are expressed as reduced mo-
5 bilities at 0°C and 1 atm, using Eq. (30). The spectra were normalized so that the area under each curve is unity. In this manner, the relative area under each peak is directly related to the relative proportion of the corresponding chemical species in the mixture.

Ions grow with time due to, essentially, clustering processes. Specifically, when there are water molecules in the system, ions grow by progressive hydration, i.e. by
10 attachment of additional water molecules. The change in mobility due to water cluster-ing is more clearly noticeable in the case of high mobility ions: addition of one water molecule to an ion results in a relatively larger growth is the ion is small. Note that neg-ative ions with mobility about 1.7 cm^2/Vs can grow into ions of mobility near 1.6 cm^2/Vs within 10 ms. The rate at which the spectra peaks shifts toward lower mobility depends
15 obviously on air humidity; mobility shifts were not so pronounced at lower water con-centrations.

In the case of positive air ions (Fig. 7) a clear shift occurs only for the ions of higher mobility. Note, however, that the relative proportion of low mobility ions (those with mobility peaks about 0.80 and 0.85 cm^2/Vs) increases with aging time, which is in
20 agreement with the qualitative picture presented above. In general, at a given fixed air humidity, the mean mobility of the ion population decreases with aging time.

Figures 8 and 9 show some mobility spectra obtained at fixed aging time and vari-able air humidity. In comparison with the previous spectra showing the effect of ion aging time, it can be observed the drastic influence that water concentration has on the
25 chemical nature of the ions. The presence of water even in trace amounts (as in the experiments in which no air was passed through the humidifier) suffices to promote wa-ter clustering (Reischl et al., 1996). Thus, for instance, the peak at 2.12 cm^2/Vs in the spectrum drawn with continuous line in Fig. 8, typical of an air ion containing a very few number of water molecules, completely disappears when air humidity rises to 15 g/m^3,

and an ion containing several more water molecules, with mobility of 1.87 cm^2/Vs, appears in its place.

The changes in mobility are less remarkable in the case of positive ions for the reason explained before: large ions do not grow relatively much. Nevertheless, the growth of low mobility positive ions into large ions is also observable as air humidity increases.

5 Conclusions

A novel, high-resolution differential mobility analyzer, specially indicated for the measurement of mobility spectra in the range 0.5–3.0 cm^2/Vs, has been developed, manufactured, and successfully tested. The novelty of the instrument resides in its parallel-plate geometry, which avoids the traditional electrode centering problem of conventional cylindrical DMAs. As with other DMAs, the apparatus described in this work permits, not only the measurement of mobility distributions, but the generation of a continuous stream of monomobile ions as well.

References

Alonso, M.: Reducing the diffusional spreading rate of a Brownian particle by an appropriate non-uniform external force field, J. Aerosol Sci., 33, 439–450, 2002.

Buryakov, I. A.: Express analysis of explosives, chemical warfare agents and drugs with multi-capillary column gas chromatography and ion mobility spectrometry, J. Chromatogr. B, 800, 75–82, 2004.

Chen, D. R., Pui, D. Y. H., Humes, D., Fissan, H., Quant, F. R., and Sem, G. J.: Design and evaluation of a nanometer aerosol differential mobility analyzer (Nano-DMA), J. Aerosol Sci., 29, 497–509, 1998.

Chen, D. R., Pui, D. Y. H., Mulholland, G. W., and Fernandez, M.: Design and testing of an aerosol/sheath inlet for high resolution measurements with a DMA, J. Aerosol Sci., 30, 983–999, 1999.

High resolution parallel plate DMA

J. P. Santos et al.

Chen, Y. H., Hill, H. H., and Wittmer, D. P.: Thermal effects on electrospray ionization ion mobility spectrometry, Int. J. Mass Spectrom., 154, 1–13, 1996.

Clemmer, D. E. and Jarrold, M. F.: Ion mobility measurements and their applications to clusters and biomolecules, J. Mass Spectrom., 32, 577–592, 1997.

de Juan, L. and Fernández de la Mora, J.: High resolution size analysis of nanoparticles and ions: running a Vienna DMA of near optimal length at Reynolds numbers up to 5000, J. Aerosol Sci., 29, 617–626, 1998.

Flagan, R.C.: History of electrical aerosol measurements, Aerosol Sci. Technol., 28, 301–380, 1998.

Hagwood, C., Sivathanu, Y., and Mulholland, G.: The DMA transfer function with Brownian motion: a trajectory/Monte-Carlo approach, Aerosol Sci. Tech., 30, 40–61, 1999.

Hill Jr., H. H. and Martin, S. J.: Conventional analytical methods for chemical warfare agents, Pure Appl. Chem., 74, 2281–2291, 2002.

Karpas, Z., Cohen, M. J.,Stimac, R. M., and Wernlund, R. F.: On the effects of structure and charge distribution on the mobility of ions, Int. J. Mass Spectrom., 74, 153–159, 1986.

Karpas, Z., Stimac, R. M., and Rappoport, Z.: Differentiating between large isomers and derivation of structure information by ion mobility spectrometry/mass spectrometry techniques, Int. J. Mass Spectrom., 83, 163–175, 1988.

Knutson, E. O. and Whitby, K. T.: Aerosol classification by electric mobility: apparatus, theory, and applications, J. Aerosol Sci., 6, 443–451, 1975.

Kousaka, Y., Okuyama, K., and Mimura, T.: Effect of Brownian diffusion on electrical classificatrion of ultrafine particles in differential mobility analyzers, J. Chem. Eng. Jpn., 19, 401–407, 1986.

Loscertales, I. G.: Drift differential mobility analyzer, J. Aerosol Sci., 29, 1117–1139, 1998.

Martínez-Lozano, P. and Fernández de la Mora, J.: Resolution improvements of a nano-DMA operating transonically, J. Aerosol Sci., 37, 500–512, 2005.

Martínez-Lozano, P., Labowsky, M., and Fernández de la Mora, J.: Experimental tests of a nano-DMA with no voltage change between aerosol inlet and outlet slits, J. Aerosol Sci., 37, 1629–1642, 2006.

Ramiro, E. and Rivero, A.: Wide range differential mobility analyzer (DMA) with very high resolution, International Patent WO 2007/020303 A1, 2007.

Reischl, G. P., Mäkelä, J. M., Karch, R., and Necid, J.; Bipolar charging of ultrafine particles in the size range below 10 nm, J. Aerosol Sci., 27, 931–949, 1996.

High resolution parallel plate DMA

J. P. Santos et al.

|◄ | ►|

◄ | ►

Back | Close

Full Screen / Esc

Printer-friendly Version

Interactive Discussion

Rosell-Llompart, J., Loscertales, I. G., Bingham, D., and Fernández de la Mora, J.: Sizing nanoparticles and ions with a short differential mobility analyzer, J. Aerosol Sci., 27, 695–719, 1996.

Rosser, S. and Fernández de la Mora, J.: Vienna-type DMA of high resolution and high flow rate, Aerosol Sci. Tech., 39, 1191–1200, 2005.

Salm, J.: Diffusion distortions in a differential mobility analyzer: the shape of apparent mobility spectrum, Aerosol Sci. Tech., 32, 602–612, 2000.

Song, D. K. and Dhaniyala, S.: Change in distributions of particle positions by Brownian diffusion in a non-uniform external field, J. Aerosol Sci., 38, 444–454, 2007.

Stolzenburg, M.: An ultrafine aerosol size distribution measuring system, Ph.D. thesis, University of Minnesota, USA, 1988.

Swing, R. G., Atkinson, D. A., Eiceman, G. A., and Ewin, G. J.: A critical review of ion mobility spectrometry for the detection of explosives and explosive related compounds, Talanta, 54, 515–529, 2001.

Tammet, H. F.: The aspiration method for the determination of atmospheric-ion spectra, Keter Press, Jerusalem, Israel, 1970.

Tammet, H., Mirne, A., and Tamm, E.: Electrical aerosol spectrometer of Tartu University, Atmos. Res., 62, 315–324, 2002.

Vautz, W., Zimmerman, D., Hartmann, M., Baumbach, J. I., Nolte, J., and Jung, J.: Ion mobility spectrometry for food quality and safety, Food Addit. Contam., 23, 1064–1073, 2006.

Whitby, K. T. and Clark, W. E.: Electrical aerosol particle counting and size distribution measuring system for the 0.015 to 1 μ size range, Tellus, 18, 573–586, 1966.

Winklmayr, W., Reischl, G. P., Lidner, A. O., and Berner, A.: A new electromobility spectrometer for the measurement of aerosols size distributions in the size range from 1 to 1000 nm, J. Aerosol Sci., 22, 289–296, 1991.

Table 1. Calculated reduced mobility for the high-mobility peak of Fig. 3. k is the mobility as calculated with Eq. (14); k_0 is the reduced mobility, calculated with Eq. (28) using the calculated values of pressure and temperature at the classification zone, shown in the second and third columns.

Q_{sh} (lpm)	P (hPa)	T (˚C)	k (cm^2/Vs)	k_0(cm^2/Vs)
215	935	22.7	2.330	1.985
292	909	19.1	2.366	1.984
370	882	16.9	2.398	1.966
447	854	14.4	2.466	1.974
515	826	12.1	2.603	2.032
607	768	8.0	2.686	1.978
671	728	6.0	2.843	1.999
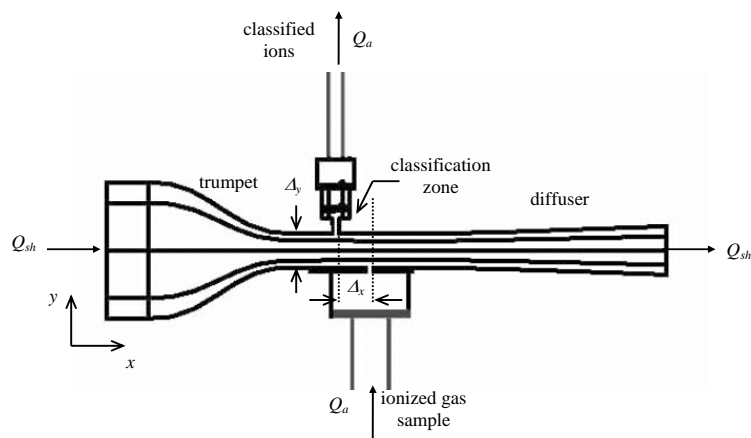
(a)
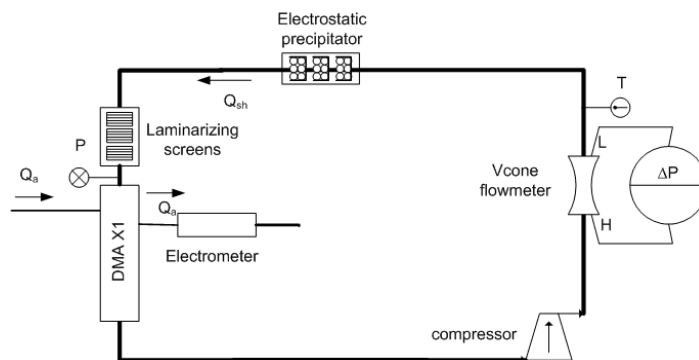
(b)

Fig. 1. Sketch of the IONER X1 Differential Mobility Analyzer: **(a)** trumpet, classification zone and diffuser; **(b)** the close-loop circuit of the sheath gas with its accessories.
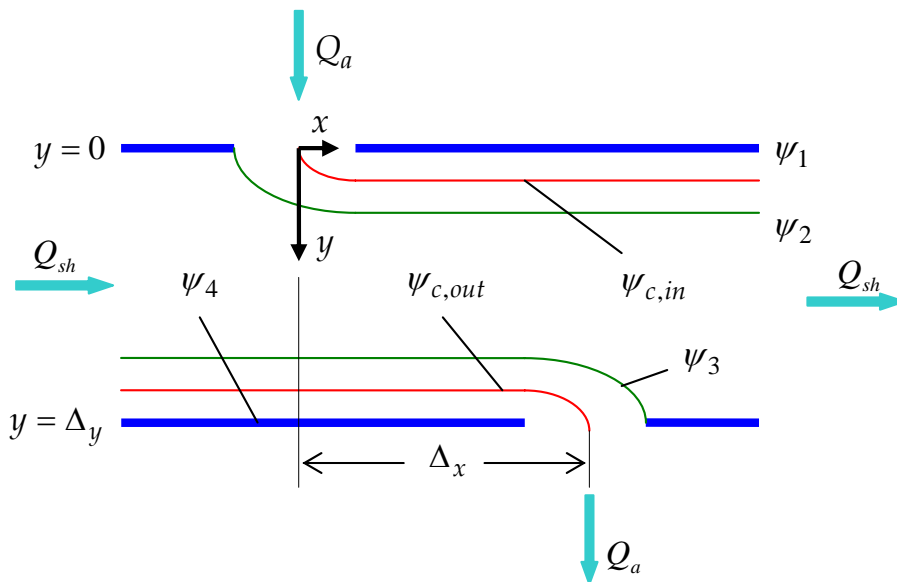
Fig. 2. Schematic representation of the streamlines involved in the determination of the DMA transfer function.

Full Screen / Esc

Printer-friendly Version

Interactive Discussion
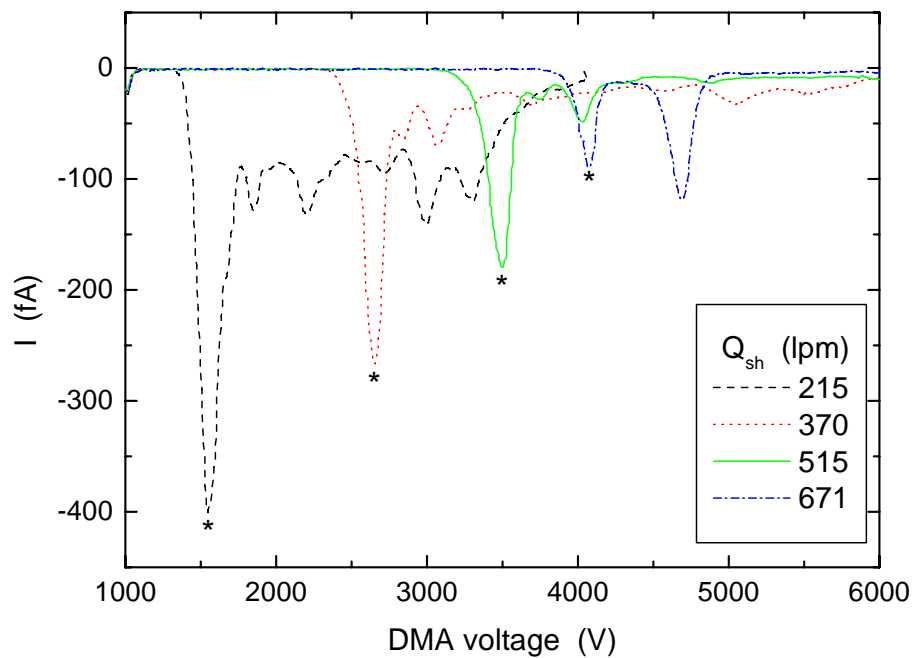
Fig. 3. Mobility spectra of negative air ions generated by corona discharge.
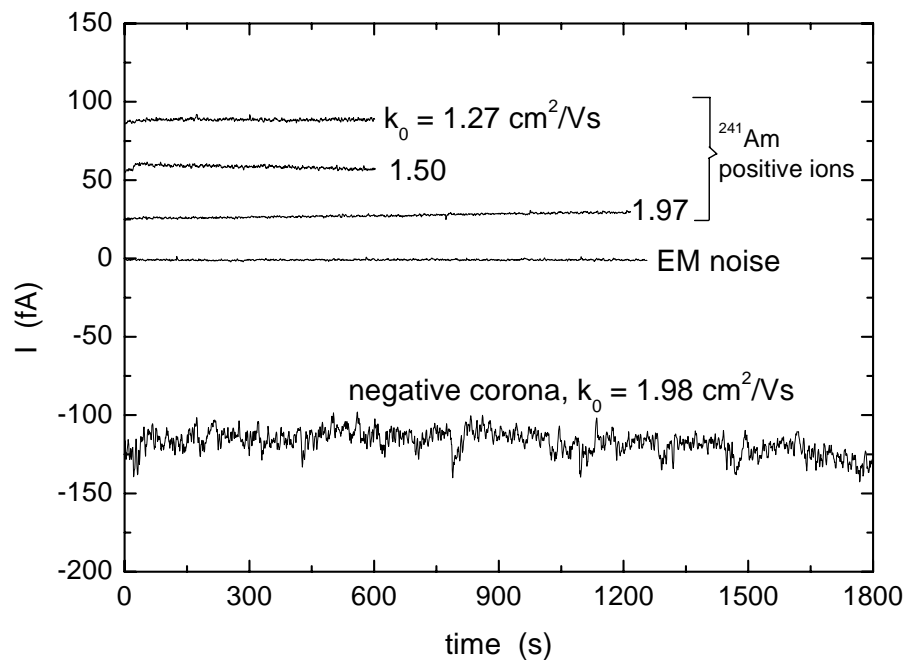
Fig. 4. Stability of DMA operating conditions and ion current measurement.
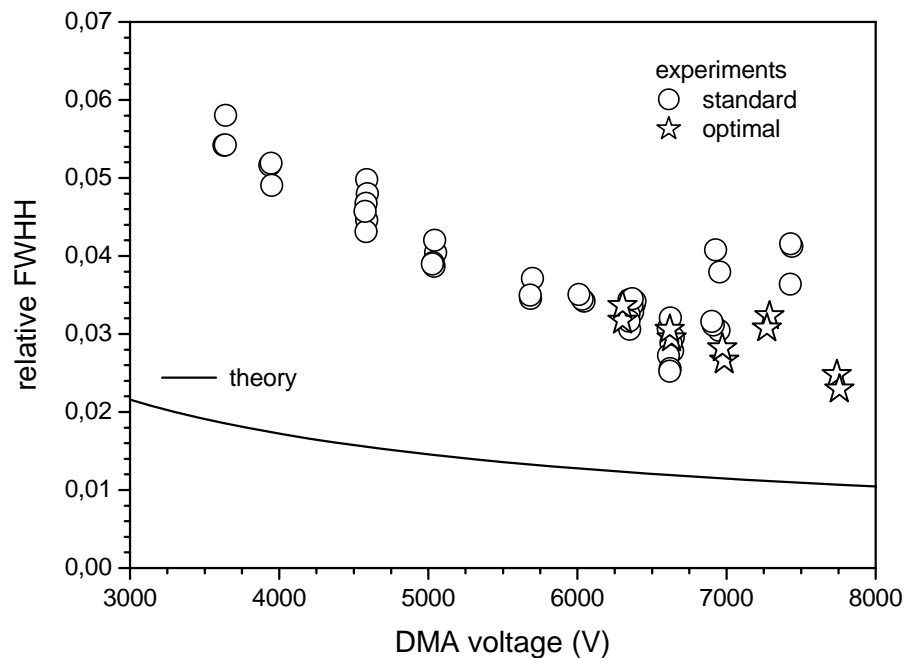
Fig. 5. Resolving power of IONER X1. Symbols: experimental results; line: curve calculated with Eq. (29).
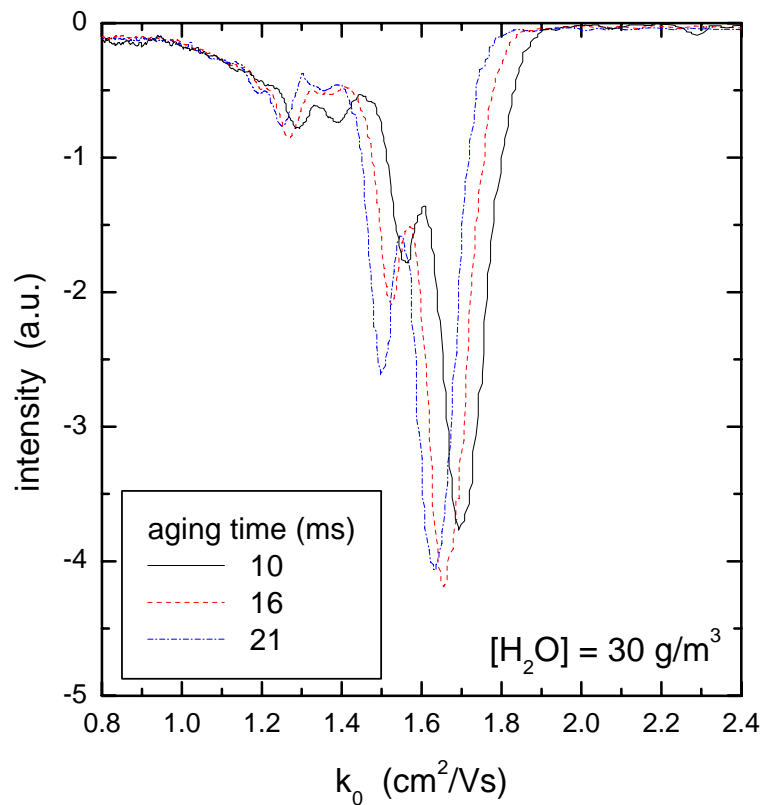
Fig. 6. Effect of aging time on the mobility distribution of negative air ions at constant humidity.
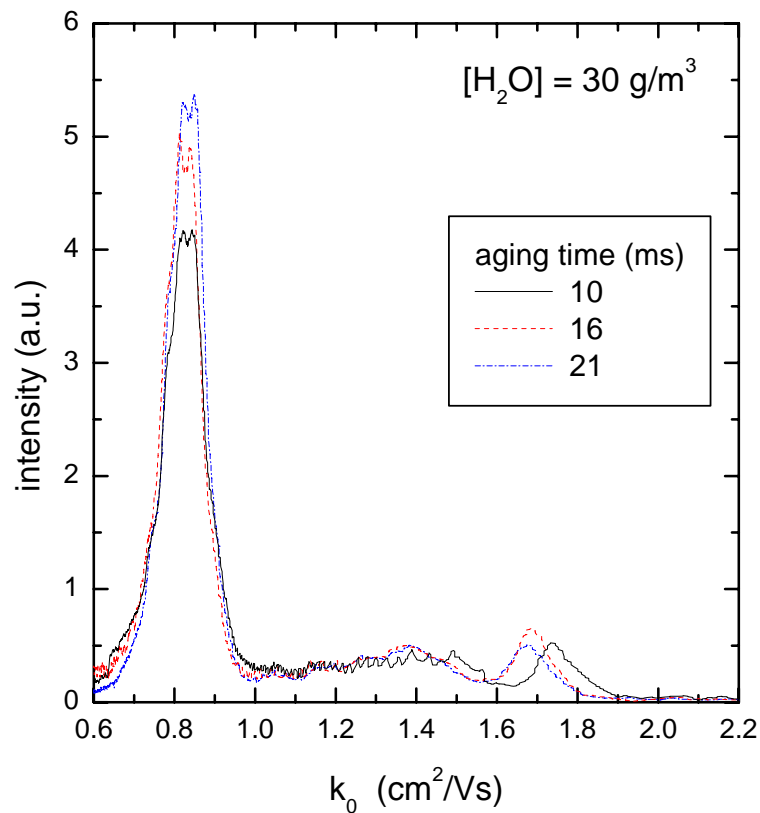
Fig. 7. Effect of aging time on the mobility distribution of positive air ions at constant humidity.
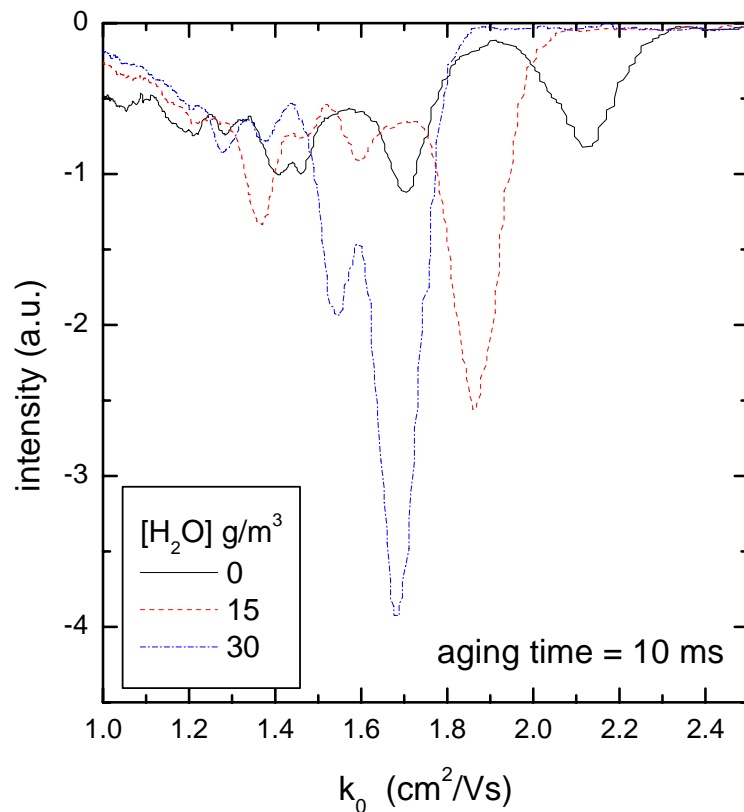
Fig. 8. Effect of air humidity on the mobility of negative air ions at fixed aging time.
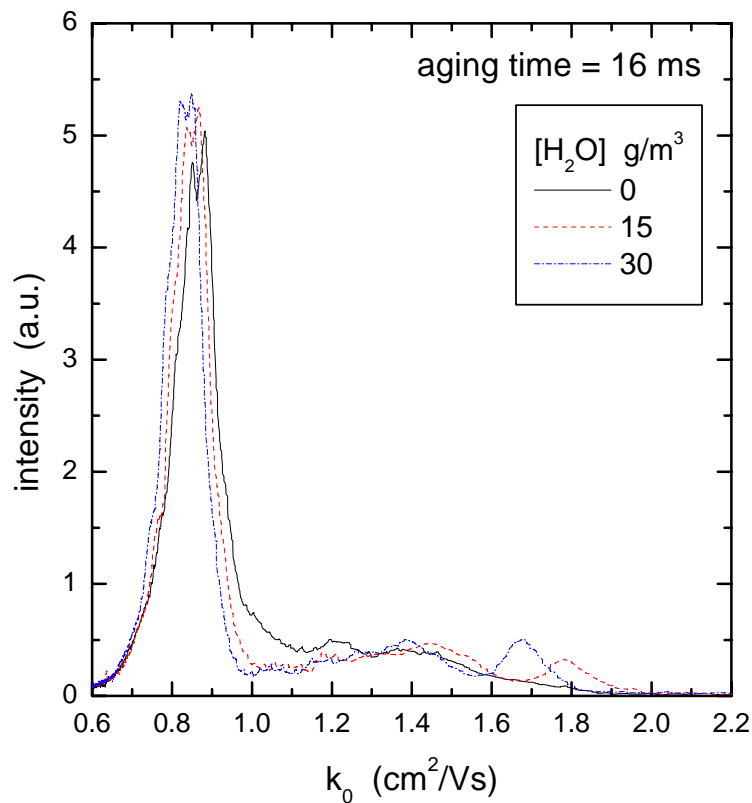
Fig. 9. Effect of air humidity on the mobility of positive air ions at fixed aging time.